Rheol Acta 38: 503–513 (1999)

ORIGINAL CONTRIBUTION

David M. Boudreau
H. Henning Winter
C. Peter Lillya
Richard S. Stein

Conoscopic observations of shear-induced rotations in nematic liquid crystals

Received: 10 December 1998
Accepted: 7 June 1999

D.M. Boudreau · C.P. Lillya · R.S. Stein
Department of Chemistry
University of Massachusetts
Amherst, MA 01003, USA

H.H. Winter (✉)
Department of Chemical Engineering
University of Massachusetts
Amherst, MA 01003, USA
e-mail: winter@acad.umass.edu

H.H. Winter · R.S. Stein
Department of Polymer Science
and Engineering
University of Massachusetts
Amherst, MA 01003, USA

Presented at EuroRheo 99-1
May 3–7, 1999, Sophia-Antipolis, France

Abstract Orientational changes in monodomains of flow-aligning liquid crystals, 4-*n*-pentyl-4′-cyanobiphenyl and *N*-(4-methoxybenzylidene)-4-butylaniline, were studied during shear and recovery in a linear shearing device fitted to an optical microscope. Planar alignment (director in the shear plane) allows the study of twist effects and was generated by strong planar anchoring at the walls with orientations in a range of 0–90° with the shear direction. While being held back by the anchoring walls, shear caused the bulk director to rotate towards a steady-state alignment angle in the shear direction (Leslie angle θ_L). The transient director rotation was observed with conoscopy. It was found that increasing the initial alignment towards the vorticity direction increased the measured θ_L. Upon stopping the flow, the bulk director returned to its initial state. With initial alignment orientation changing from parallel to perpendicular to the flow direction, the rate of the twist-driven recovery process increases. This rate increase is not seen in the splay-driven recovery which is constant and consistently faster than twist-driven recovery at all orientations studied.

Key words Monodomain · Conoscopy · Alignment angle · Shear

Introduction

Under shear flow, planar monodomains of nematic liquid crystals (LCs), initially oriented in the flow direction, will either rotate against vorticity and assume a steady-state alignment angle or they will rotate with the vorticity of the flow and develop an instability depending upon the strain rate applied (Gähwiller 1972; Pieranski and Guyon 1974; Skarp et al. 1979), as predicted by Leslie (1966) and Ericksen (1960, 1962).

Two parameters, **n** and S, express the local state of molecular orientation and order, respectively, in nematic liquids. The director **n** defines the average molecular alignment direction. It is a unit vector which, in polar coordinates, is locally defined by its angle ϕ with the vorticity plane and its angle θ with the shear plane, see Fig 1. Variations in molecular orientation around **n** are expressed by the order parameter S, where $S=0$ corresponds to random molecular orientation and $S=1$ is perfect alignment with **n** (de Gennes and Prost 1993).

The order in LC materials is far from being prefect with S being well below 1, as exemplified by 4-*n*-pentyl-4′-cyanobiphenyl (5CB) with $S=0.53$ (Madhusudana and Pratibha 1982), and *N*-(4-methoxybenzylidene)-4-butylaniline (MBBA) with $S=0.64$ (Kirov et al. 1980) at 25 °C. S decreases with increasing temperature and drops to zero above the nematic to isotropic transition.

Leslie (1966) and Ericksen (1960, 1962) proposed a continuum theory for ideal LCs during flow. For such continuous monodomain samples, six viscosity coefficients ($\alpha_1, \ldots, \alpha_6$), five independent and one dependent (Parodi 1970), determine the director orientation when disturbed by an external force such as shear or applied electric and magnetic fields. Three additional elastic constants K_1, K_2, and K_3 (splay, twist, and bend) come into play when orientational gradients are introduced

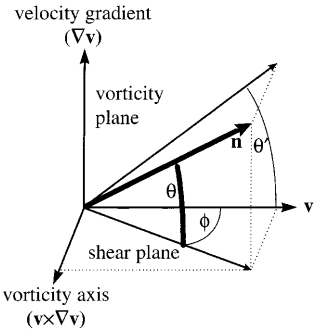

Fig. 1 Director orientation can be characterized by two polar angles. A ϕ-rotation is the rotation of the director as observed in the shear plane, while a θ-rotation denotes the director tilt out of the shear plane. To evaluate the rotation in the vorticity plane (θ'), **n** is projected into that plane. The relation between θ and θ' is $\tan\theta' = \tan\theta/\cos\phi$

across the sample (de Gennes and Prost 1993). When a monodomain is sheared at a constant rate, the LC director rotates until it assumes a constant angle θ_L (Leslie angle) with the shear planes. In the theoretical case, when there are no anchoring surfaces and the elastic contributions of boundary effects are thus nonexistent, the Leslie angle is predicted as,

$$\tan\theta_L = \sqrt{\alpha_3/\alpha_2} \tag{1}$$

given the values of the viscosity coefficients α_2 and α_3, where $\alpha_3/\alpha_2 > 0$. This prediction is independent of shear rate and independent of the initial alignment direction $\mathbf{n}_0$ as long as no orientational gradients exist across the sample. The Ericksen transversely isotropic fluid model (Ericksen 1960, 1962) has been applied to the start-up of shear flow at constant rate $\dot{\gamma}_0$, where it predicts the rotation of the director as a function of time and the shear rate in the two-dimensional (2-D) case neglecting boundary effects (i.e. $\phi = \phi_0 = 0°$; Carlsson 1984):

$$\frac{\tan\theta(\gamma) - \tan\theta_0}{\tan\theta_L - \tan\theta_0} = \frac{\exp\left(\frac{\gamma}{\gamma_L}\right) - 1}{\exp\left(\frac{\gamma}{\gamma_L}\right) + 1}; \quad \gamma_L = \frac{1 - \tan^2\theta_L}{2\tan\theta_L} \tag{2}$$

The applied strain being $\gamma = \dot{\gamma}_0 t$. In the case of Eq. (2), γ_L is the material characteristic strain at which 46% of the rotation is complete. The transient angle $\theta(\gamma)$ is predicted from θ_L; no further parameter is needed or allowed. Equation (2) applies to flow-aligning molecules, for which α_3/α_2 is positive. Otherwise ($\alpha_3/\alpha_2 < 0$), no steady-state alignment angle would be achieved in these situations; instead, the director would continually rotate in the direction of vorticity of the shear flow until instabilities set in. This experimental study is only concerned with flow-aligning systems.

As stated above, Eqs. (1) and (2) neglect the constraints on director rotation attributed to the anchoring walls of a flow cell. Anchoring may introduce a splay and twist gradient which gives rise to elastic effects. At low shear rates, these elastic effects play a dominant role in director rotation. As the shear rate increases, the splay and twist gradient associated with anchoring decreases in thickness until its impact on the bulk is negligible. The ratio of the viscous to the elastic contributions to director rotation is expressed in the Ericksen number, see for instance Larson (1999):

$$\mathrm{Er} = \frac{\alpha_3 - \alpha_2}{K_1} h^2 \dot{\gamma} \ . \tag{8}$$

When $\mathrm{Er} \gg 1$, boundary effects are negligible as viscous torques from shear far outweigh the elastic torques from anchoring; only then can Eqs. (1) and (2) be applied reliably.

Monodomain samples have a relatively high order parameter and a reasonably uniform director over a large scale. Therefore, experiments with monodomains can be used to approximate most closely the orientational conditions used by the Ericksen TIF model. They also provide a high enough director orientation to allow the use of conoscopy.

Conoscopy can be used to measure the average director orientation throughout a sample by taking advantage of the high birefringence or ordered LCs. Focusing a highly convergent beam of polarized monochromatic light onto an LC monodomain generates an interference pattern in the back focal plane of a microscope objective. Details of the formation of the conoscopic image can be found in various texts (Bloss 1961; Born and Wolf 1969; Wahlstrom 1969).

Conoscopy allows separate measurement of the average director angle ϕ and θ, but certain factors must first be taken into account. In an ideal sample, the director is oriented uniformly across the sample thickness. A conoscopic image from this sample would express the director's true orientations. Real samples have director gradients due to wall effects. During shear flow, the local director adjacent to the anchoring walls remains relatively fixed while the bulk director rotates towards the Leslie angle resulting in a splay gradient. If the director at the anchoring walls is oriented at an angle ϕ_0 to the shear direction, a twist gradient exists in addition to the splay.

The resulting conoscopic interference pattern averages the director orientation over the sample thickness.

$$\phi_{ap} = \frac{1}{h}\int_0^h \phi(y)\mathrm{d}y; \quad \theta_{ap} = \frac{1}{h}\int_0^h \theta(y)\mathrm{d}y \tag{3}$$

Because of this, the apparent rotation of the conoscopic figure (ϕ_{ap}) is less than the rotation of the director at the sample midplane (ϕ). The discrepancy between these values increases as the difference between ϕ and ϕ_0 increases. Cladis (1972) addressed this problem by defining an apparent rotation,

$$\tan 2\phi_{ap} = \frac{2\sin\phi}{2E(\pi/2, \sin\phi) - F(\pi/2, \sin\phi)} \quad (4)$$

where $F(\pi/2, \sin\phi)$ and $E(\pi/2, \sin\phi)$ are the complete elliptic integrals of the first and second kind, respectively. Srinivasarao and Berry (1991) approximated the rotation angle in Eq. (4) with Eq. (5). This allows the easy calculation of ϕ when ϕ_{ap} is known to within 3%, since $|\phi - \phi_0| < 90°$.

$$\phi \approx \frac{\pi/2\phi_{ap}}{1 + 0.14\phi_{ap}^2} \quad (5)$$

The apparent director rotation out of the shear plane (θ-rotation), for a sample with initial planar alignment is calculated with Eq. (6) (Tobi 1956; Srinivasaro and Berry 1991). The angle (θ_{ap}) is determined by the ratio of the displacement of the center of the

$$\sin\theta_{ap} = \frac{r}{R}\frac{NA}{\langle n\rangle} \quad (6)$$

conoscopic fringe pattern (r) to the radius of the whole image (R). NA and $\langle n\rangle$ are the numerical aperture of the microscope objective and the average index of refraction of the sample, respectively. θ_{ap} is the angle that marks the path of minimum phase difference through the sample. For homeotropic alignment, the path of minimum phase difference is nearly parallel to the optic axis of the sample and θ_{ap} equals the angle of the director. In the case of planar orientation, θ_{ap} must be converted to the actual average director splay angle ($\langle\theta\rangle$),

$$\langle\tan\theta\rangle = \frac{\sin 2\theta_{ap}}{3 + \cos 2\theta_{ap}} \quad . \quad (7)$$

As long as the conoscopic image center remains in the field of view ($r \leq R$) the combination of Eqs. (6) and (7) can be employed reliably, assuming that the effects of the ϕ and θ rotations on the conoscopic image are independent of each other.

Conoscopy is an established tool for studying LC orientation. Early work determined a steady-state alignment angle, $\theta_\infty(\phi_0)$, either by counting the number of fringes observed under the conoscope during shear (Wahl and Fischer 1973; Skarp et al. 1979) or by counting the number of fringes passing a fixed point from the start-up of shear (Gähwiller 1972; Pieranski and Guyon 1973). The work of Pieranski and Guyon is particularly interesting for their initial alignment conditions. LC samples were placed between parallel glass plates that were coated with a SiO film. This film, along with a magnetic field, induced the planar alignment of a sample of MBBA along the vorticity axis ($\phi_0 = 90°$, $\theta_0 = 0°$). They found that a critical shear rate was necessary before the director would undergo a ϕ-rotation and orient towards the velocity direction. The evolution of $\theta(t, \mathrm{Er}, \phi_0)$ was not commented upon but the $\theta_\infty(\phi_0)$ values obtained seem to correspond well with the experimental observations of Gähwiller (1972), being only a few degrees larger with $\theta_\infty(\phi_0) \cong 10°$. In more recent work, Hongladarom and Burghardt (1994) measured the full refractive index tensor and determined the molecular orientation of a sheared polymer solution by using a variation of the conoscopic technique which focuses on specific light paths within the cone of light. Other works include Mather et al. (1996) and Müller et al. (1994, 1996a, 1996b) who followed the movement of the center of the conoscopic image during shear. These techniques allow a more direct determination of the θ component of the director rotation.

It is the goal of this research to observe the time-dependent evolution of the alignment angle in small molecule nematic LC monodomains perturbed by shear. The initial planar alignment conditions of Müller et al. (1994), with the director oriented along v ($\phi_0 = 0°$, $\theta_0 = 0°$), and Pieranski and Guyon (1974), with the director oriented along $\mathrm{v} \times \nabla\mathrm{v}$ ($\phi_0 = 90°$, $\theta_0 = 0°$), are studied with intermediate planar alignment conditions where $0° \leq \phi_0 \leq 90°$.

We wish to observe the effect that the twist, prescribed by the anchoring at the boundary surface, has on the ϕ-rotation and θ-rotation of the director during shear and recovery. During shear the evolution of the rotation angles $\theta(t, \mathrm{Er}, \phi_0)$ and $\phi(t, \mathrm{Er}, \phi_0)$, and their dependence on time, shear rate, and initial alignment angle are measured as well as their steady-state alignment angles at long times $\theta_\infty(\mathrm{Er}, \phi_0)$, $\phi_\infty(\mathrm{Er}, \phi_0)$. The maximum steady-state alignment angles, $\theta_\infty(\phi_0)$, $\phi_\infty(\phi_0)$, which are independent of the Ericksen number are studied as well. $\theta_\infty(\phi_0 = 0°)$ will then be compared to the ideal case of the Leslie angle (θ_L) of Eqs. (1) and (2).

The angles $\theta_r(t, \phi_0)$ and $\phi_r(t, \phi_0)$ are observed during recovery of the monodomain after the cessation of shear. The recovery should be dependent upon the initial alignment conditions since the twist and splay gradients in the boundary layers, as governed by the elastic constants K_1, K_2, and K_3, provide the driving force for the director rotation.

Experimental

The materials used in this experiment are two low molecular weight nematics: MBBA and 5CB (Aldrich Chemical). Shear-induced director rotation was studied with both materials, while recovery studies involved only MBBA.

LC samples were placed between two $25 \times 75 \times 1$ mm glass slides separated by 150-μm-thick glass spacers. Prior to use, the glass slides were each coated with a 0.1-μm-thick polyimide resin layer and then buffed at angles of $\phi_0 = 0°$, 22.5°, 45°, 67.5° and 90° with respect to the shear direction. The buffing produces molecular alignment at the polyimide surface that strongly anchors the LC molecules in the direction of the rubbing. This surface alignment then propagates through the bulk of the sample (Nejoh 1991).

The Zeiss optical microscope used for observing the conoscopic interference patterns was equipped with a condensing lens of focal length 1 mm, a 40× objective with a 0.75 numerical aperture, an Amici-Bertrand lens, and a polarizer and analyzer angled ±45° to the shear direction. The light source for the experiment was a 30 mW, 632.8 nm HeNe laser. No expansion of the laser beam was used.

Samples mounted on the microscope stage were sheared by translation of the lower glass plate by an inchworm motor (Burleigh) capable of speeds $v = 0.5\ \mu m\ s^{-1}$ to $4000\ \mu m\ s^{-1}$. The sample thickness of $h = 150\ \mu m$ permits shear rates of $3 \times 10^{-3}\,s^{-1} < \dot{\gamma} < 10\,s^{-1}$, where $\dot{\gamma} = v/h$, and a total strain of $\gamma = 60$. Higher rates than these could possibly be obtained by decreasing the sample thickness but this would consequently increase the role that the boundary layer plays in the observed conoscopic image. Experiments were conducted at 25 °C and at constant shear rates which ranged from $\dot{\gamma} = 0.078\,s^{-1}$ to $8.2\,s^{-1}$. After shearing between t_0 and t_1, the flow was stopped and gradual recovery of the initial alignment was observed at times $t > t_1$. The time evolution of conoscopic images was collected on videotape and then transferred to a computer. For evaluation of θ_{ap}, the center of the fringe pattern was determined by measuring four points on the image. Each point marked the center of a hyperbolic fringe and its counterpart, thus defining a cross with its center at the center of the pattern (measured in units of pixels). The angle that the cross makes with the image horizontal gives the angle ϕ_{ap}.

Results

First, the effect of any pre-tilt orientation on the measured steady-state alignment angle was studied (Weiss et al. 1998). A sample of MBBA was placed between glass slides rubbed in opposite directions relative to the sample. This rubbing produced a symmetric +2°, +2° pre-tilt angle at the walls and $\theta_0 \approx 2°$. The sample was sheared in two directions until a steady-state alignment angle was observed in each direction. The conoscopically observed angle was the same in each case.

An asymmetric anchoring of +2°, −2° was then prepared. This allowed for the tilt bias of one anchoring surface to cancel out the tilt bias of the other surface, when averaging over the optical light path through the sample ($\theta_0 = 0°$). Upon shearing, the observed steady state alignment angle was the same as for the symmetrical anchoring. Therefore the glass buffing which produced no observable pre-tilt angle was chosen for the remainder of the experiment.

Figure 2 shows a series of typical conoscopic images as seen through the microscopic between cross polars. The fixed ring in the center of the images is a consequence of the objective used and has no bearing on the measurements. The example in Fig. 2 was chosen to show both translation and rotation of the image with increasing strain.

The translation of the fringe pattern at various shear rates (Ericksen numbers) is analyzed in Fig. 3. It shows the evolution of the average values of $\theta(t, \mathrm{Er}, \phi_0)$ during the shearing of MBBA. The results for 5CB are similar. In all the experiments of this study, the average director is initially in the shear plane, $\theta_0 \approx 0°$. The boundary layer effect is reflected in the low steady-state alignment angles at lower Ericksen numbers. The lowest Ericksen number used produces an average steady-state alignment angle $\theta_\infty(\mathrm{Er}, \phi_0)$ of 3.47 ± 0.09° for MBBA. This angle increases with increasing shear rate as the contribution from the boundary layers diminishes. Eventually a point is reached at high enough Ericksen numbers where the boundary layer effect is no longer obvious. This is seen in Fig. 3 for Er > 450 where the steady-state alignment angle becomes independent of the strain rate, $\theta_\infty(\phi_0)$. Figure 4 also shows this result where, at high values of Er, $\theta_\infty(\mathrm{Er}, \phi_0)$ reaches a plateau.

Proceeding to Fig. 3 middle and bottom, a finite initial alignment angle, ϕ_0, introduces a retardation period at the start-up of shear. This is most prominent for $\phi_0 = 90°$, Fig. 3 (bottom). The maximum average steady-state alignment angle, $\theta_\infty(\phi_0)$, although independent of Er, was found to be dependent on the initial alignment direction. Figure 4 shows that as ϕ_0 is increased, the steady-state alignment angle at any given Ericksen number is also increased. This is prominent even at high Er values where for MBBA, $\theta_\infty(\phi_0)$ increases from 7.6°, to 9.1° to 9.7° with $\phi_0 = 0°$, 45° and 90° respectively.

Figure 5 shows the evolution of the rotation in the shear planes, $\phi(t, \mathrm{Er}, \phi_0)$, during the shearing of MBBA. At $\phi_0 = 0°$ the director is already oriented in the shear direction and no ϕ-rotation is observed (Fig. 5b, top). With $\phi_0 > 0°$, the director rotates into the shear direction (Fig. 5b, middle and bottom) given that the

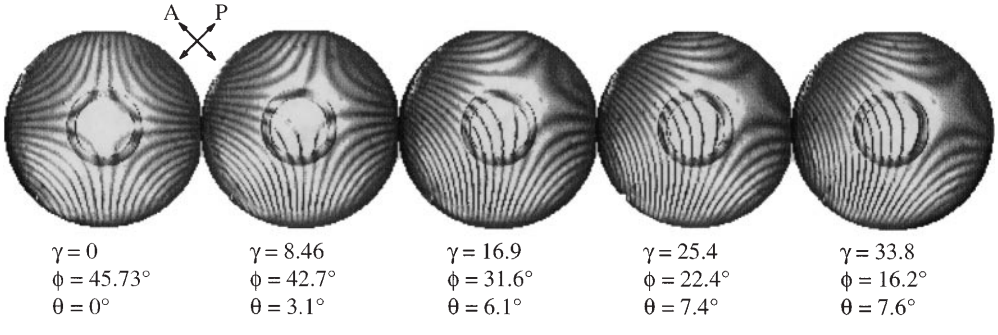

Fig. 2 Conoscopic images from MBBA initially oriented at $\phi_0 = 45°$; $\theta_0 = 0°$ and sheared at 1.69 s^{-1} (Er = 2240). Images are at 5 s intervals starting at $t = 0$. The ring in the center of the conoscopic image is an artifact of the Ph2, 40/0.75 W, 160/-objective used

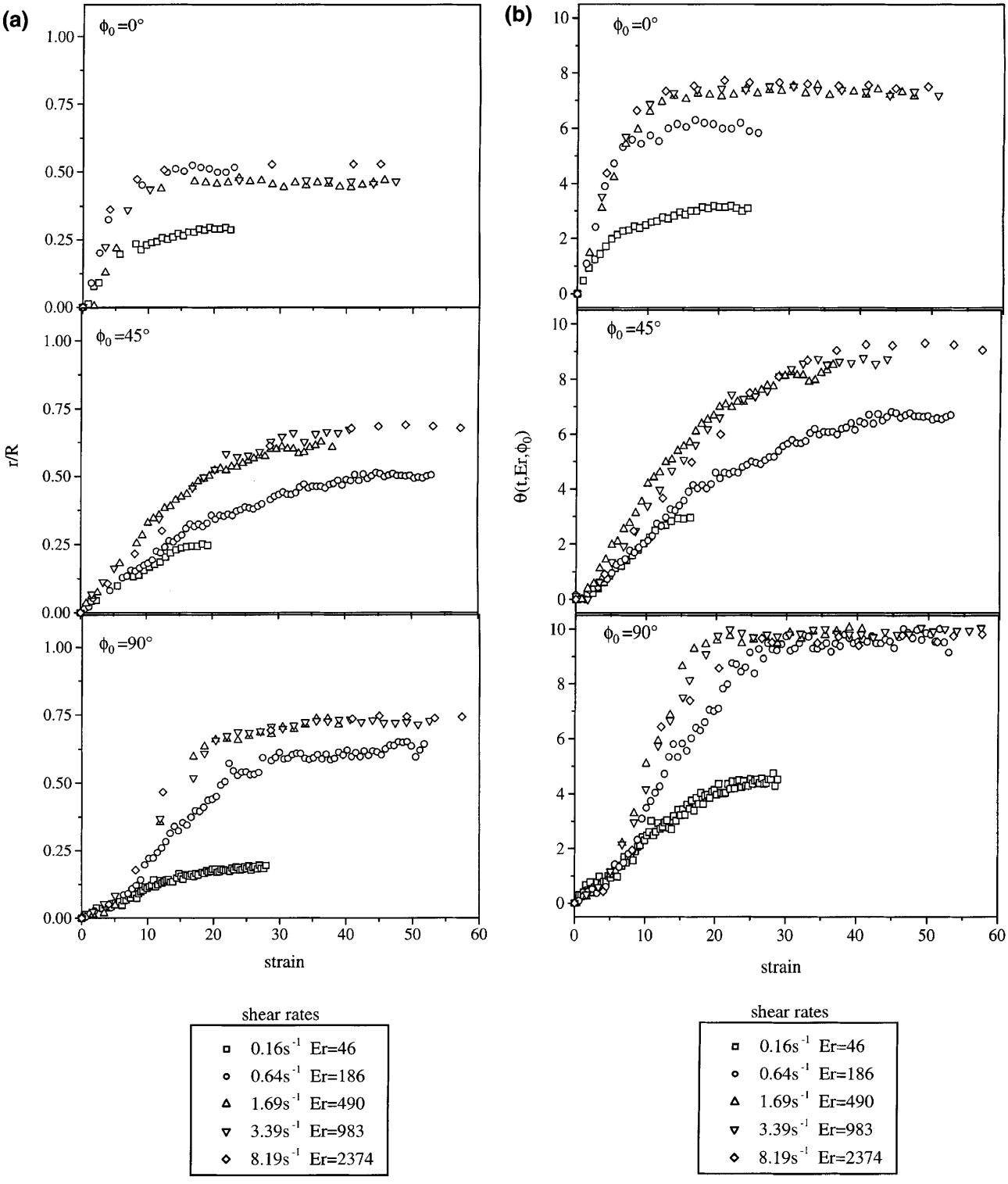

Fig. 3 a Values of r/R obtained from the conoscopic image of sheared MBBA with $\theta_0 = 0°$, and initial alignment angle $\phi_0 = 0°$, 45°, and 90° respectively. **b** Evolution of θ-rotation for MBBA starting with planar alignment $\theta_0 = 0°$, and initial alignment angle $\phi_0 = 0°$, 45°, and 90° respectively

shear rate is high enough to overcome the boundary effects.

The trends seen in MBBA also exist for 5CB. Although the same shear rates were used for both

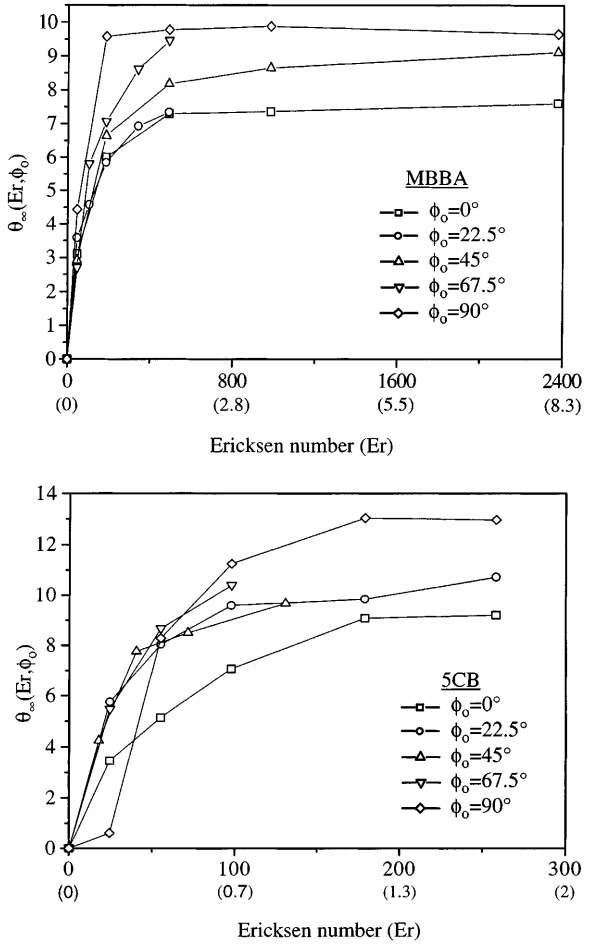

Fig. 4 Maximum steady-state alignment angles of MBBA and 5CB for director splay from various initial alignment conditions. The values in parentheses are the corresponding shear rates (s^{-1}). θ_∞ becomes independent of shear rate at high Ericksen values

MBBA and 5CB, the Ericksen numbers are much lower for any given rate with 5CB (Fig. 4, bottom). Therefore, the results for 5CB must also take into account a greater influence by the boundary layer. This influence would explain features observed with 5CB but not with MBBA. First, even though curves for 5CB were similar in shape to those of Fig. 3, the transient portion of the curves had differing slopes even when a common steady-state value was reached at high shear rates. If the boundary effects were insignificant, then these transients should be independent of shear rate. Secondly in Fig. 4 (bottom), the lowest shear rate used with $\phi_0 = 90°$, produces almost no splay rotation resulting in $\theta_\infty(\mathrm{Er},\ \phi_0) = 0.6° \pm 0.1°$. This special case of very low Ericksen numbers and $\phi_0 = 90°$ was studied by Pieranski and Guyon (1973). They noticed that a critical Ericksen value was necessary to force the director to rotate out of the vorticity direction. Below this critical value, the anchoring effects of the boundary layer play such a dominant role that no director rotation is observed (Manneville and Dubois-Violette 1976).

At time $t = t_1$, the flow was stopped and the samples of MBBA were allowed to relax from their shear-induced orientation by recovering the initial monodomain state. The steady-state alignment angles obtained during shear, $\theta_\infty(\mathrm{Er},\ \phi_0)$ and $\theta_\infty(\mathrm{Er},\ \phi_0)$, are the starting values for the recovery process. Due to the strong surface anchoring, the director reorients into the shear plane, $\theta_0 = 0°$, and to the initial alignment angle ϕ_0. Figure 6 shows the splay-induced recovery, $\theta_r(t,\ \phi_0)$ after the cessation of shear at t_1 where the initial alignment of the sample was $\phi_0 = 0°$, 45°, and 90° respectively.

The twist-induced recovery, $\theta_r(t, \phi_0)$, from $\theta_\infty(\mathrm{Er},\ \phi_0)$ back to ϕ_0, is shown in Fig. 7. For the cases where $\phi_0 = 45°$ and $\phi_0 = 90°$, Fig. 7(middle and bottom), ϕ-recovery follows a simple exponential function. Figure 7(top) is only shown for completeness; there is obviously no rotation in the shear plane since the steady-state alignment angle, $\theta_\infty(\mathrm{Er},\ \phi_0)$, is approximately equal to the initial value of ϕ_0.

Discussion

The θ-rotation and θ_∞ obtained in our study are now compared with the Ericksen TIF model, Eqs. (1) and (2). According to the model, the director rotates out of the shear plane with the onset of shear. Immediately with the beginning of shear, the rotation starts at a rate

$$\left(\frac{\mathrm{d}\theta}{\mathrm{d}t}\right)_0 = \theta_\mathrm{L}\frac{\dot{\gamma}}{\gamma_\mathrm{L}} \quad . \tag{8}$$

The rate of rotation decreases until the director reaches its maximum steady-state alignment angle (Leslie angle). The 2-D model does not include any ϕ-rotation of the director out of the vorticity plane nor does it include the boundary effects introduced by the walls of the shear cell. Because of these idealizations in the model, deviations of the experimental observations may be expected.

A fitting function was chosen that would accurately express the measured behavior of $\theta(t, \mathrm{Er}, \phi_0)$ for $0° \le \phi_0 \le 90°$. Equation (9) is a curve-fitting sigmoidal Weibull function (Weibull 1951) that has been modified to reflect Eq. (2) more closely.

$$\frac{\tan\theta(t,\mathrm{Er},\phi_0) - \tan\theta_0}{\tan\theta_\infty(\mathrm{Er},\phi_0) - \tan\theta_0} = \frac{\exp\left[\left(\frac{\gamma}{\chi\gamma_{\mathrm{L}\,\mathrm{exp}}}\right)^m\right] - 1}{\exp\left[\left(\frac{\gamma}{\chi\gamma_{\mathrm{L}\,\mathrm{exp}}}\right)^m\right] + 1} \tag{9}$$

The amount of director rotation $\theta(t, \mathrm{Er}, \phi_0)$ which is dependent upon time, Ericksen number, and initial alignment angle can be expressed in terms of the steady-state alignment angle, $\theta_\infty(\phi_0)$, strain, and the parameters

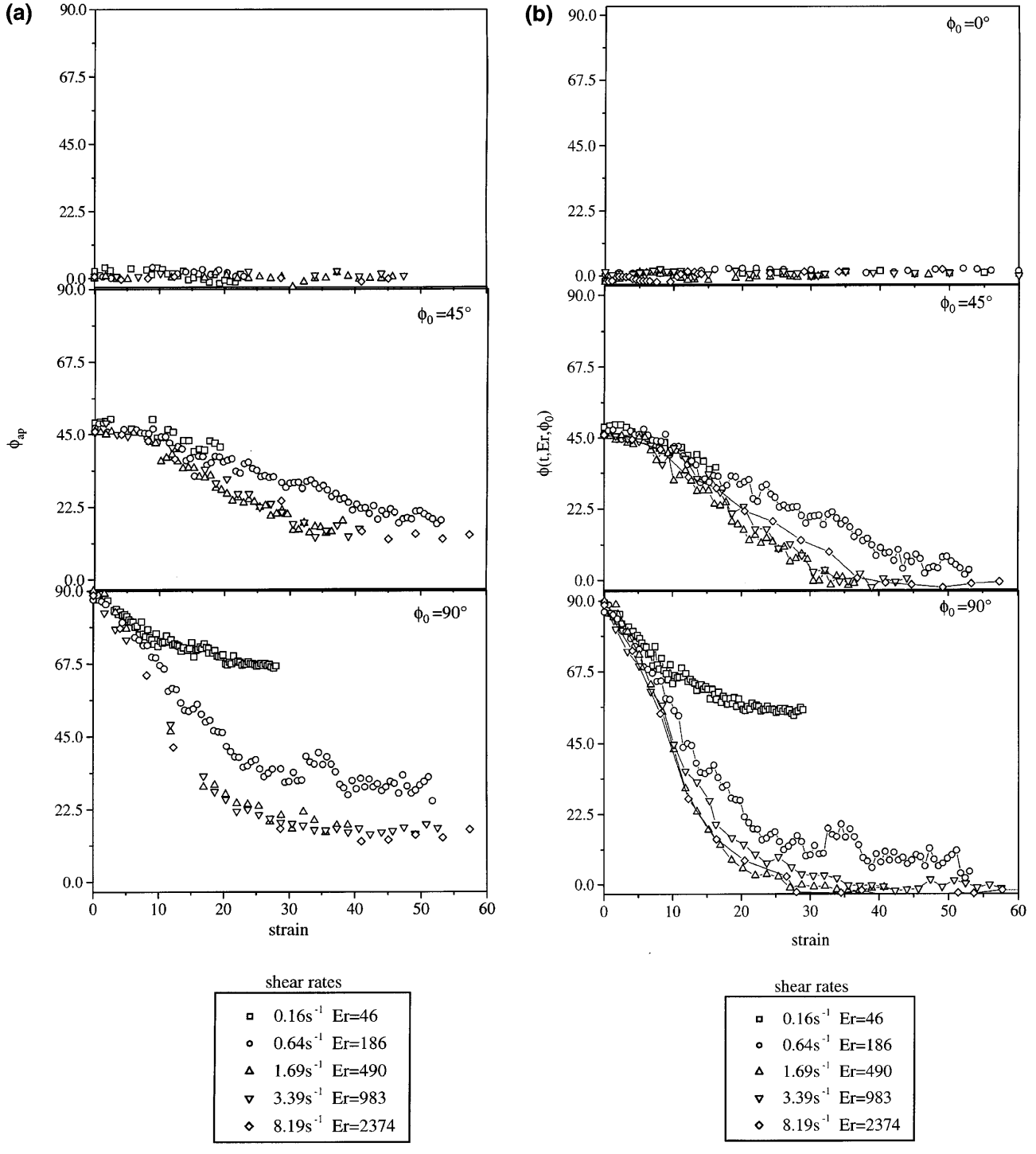

Fig. 5 a Values of ϕ_{ap} obtained from the conoscopic image of sheared MBBA with $\theta_0 = 0°$, and initial alignment angle $\phi_0 = 0°$, 45°, and 90° respectively. **b** Evolution of director ϕ-rotation for MBBA starting with planar alignment $\theta_0 = 0°$, and initial alignment angle $\phi_0 = 0°$, 45°, and 90° respectively

γ_{Lexp}, m, and χ. The variables m and χ are functions of the initial alignment conditions. χ accounts for the retardation period at the onset of shear associated with increasing ϕ_0, and m relates to the slope of the director transient. All parameters were fit to the experimental data using a least squares approach. Figure 8 shows plots of the fitting parameters χ and m versus the initial alignment angle.

In the specific condition when $\phi_0 = 0°$ and $\theta_0 = 0°$, the variables $m(\phi_0)$, and $\chi(\phi_0)$, should both equal 1. In this

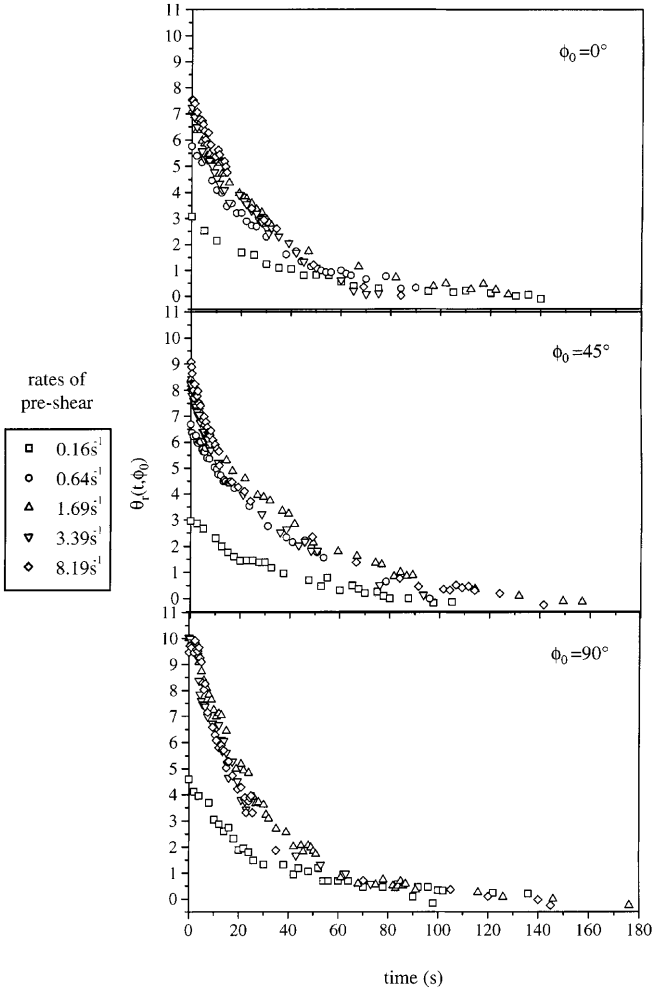

Fig. 6 Splay-induced recovery of the director for MBBA back to the initial alignment angles of $\theta_0 = 0°$, and $\phi_0 = 0°$, 45°, and 90° respectively. The shear rates refer to the shearing prior to recovery

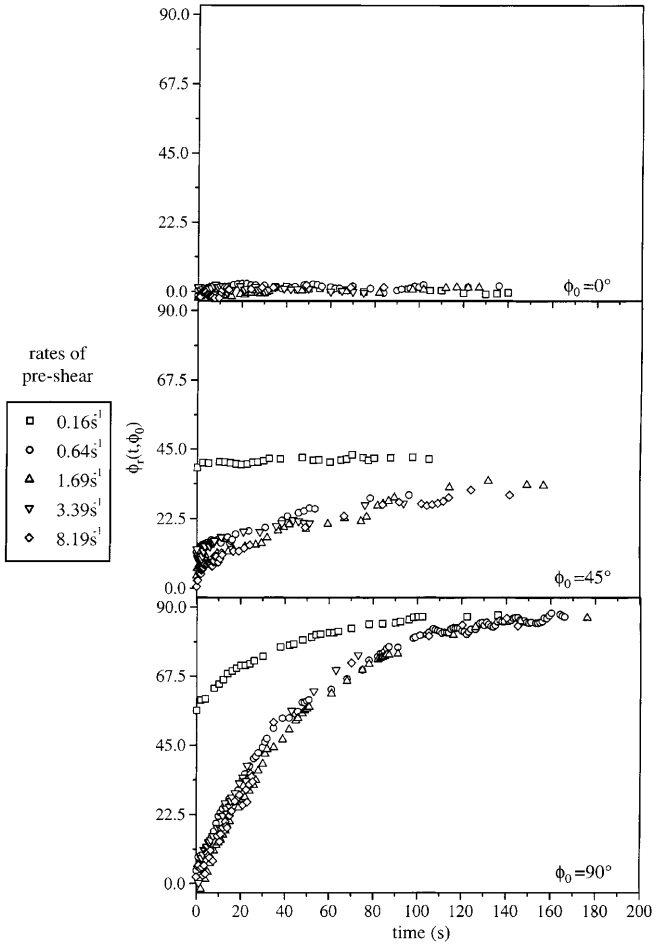

Fig. 7 Twist-induced recovery of the director for MBBA back to the initial alignment angles of $\theta_0 = 0°$, and $\phi_0 = 0°$, 45°, and 90° respectively. The shear rates refer to the shearing prior to recovery

situation Eq. (9) reduces to Eq. (2) of the Ericksen TIF model. This means that if the maximum observed steady-state alignment angle of our experiments is really the Leslie angle of Eq. (2) then the curve-fitted γ_{Lexp} must equal γ_{L} as calculated by the second part of Eq. (2). Figure 9 assumes that $\theta_\infty(\phi_0) = \theta_{\mathrm{L}}$. With this assumption, a value for γ_{L} is calculated based upon $\theta_\infty(\phi_0)$ and compared to the curve fit using the experimentally determined γ_{Lexp}. The points represent data from the highest Ericksen number used. The solid curves represent the upper and lower limits of the curve fit based upon $\theta_\infty(\phi_0)$, and a least squares fit of γ_{Lexp}, $\chi \approx 1$, $m \approx 1$. The dotted lines show the limits when γ_{L} is specifically calculated from $\theta_\infty(\phi_0), \chi = 1, m = 1$.

Figure 9 (top) shows that for MBBA there is very good agreement between the experimental γ_{Lexp} and γ_{L} with the two values being within experimental error. This means that the higher shear rates used were enough to limit the anchoring effects of the sample walls. The same technique is applied to 5CB in Fig. 9 (bottom). As can be seen, there is a poor fit between the experimental $\gamma_{0.46}$ and calculated γ_{L} with the calculated value being almost double the experimental value. This is most probably due to the shear rate producing a low Ericksen value of only 188. Boundary effects greatly influence the observed $\theta_\infty(\phi_0)$ and the model does not account for boundary effects in the transient portion of the curve.

Table 1 compares the Leslie angles obtained here in our experiments with the work of others. The results of $\theta_\infty(\phi_0 = 0°)$ from this study correspond well with the previous work of others for MBBA but, due to the low Ericksen numbers used, 5CB has a relatively low value in comparison to the majority of published work.

In the cases where $\phi_0 \neq 0°$, various effects were seen on θ-rotation during shear. First χ increases with increasing initial alignment angle as shown in Fig. 8 (top). This means that a retardation of the θ-rotation sets in as the initial alignment tends towards $\phi_0 = 90°$.

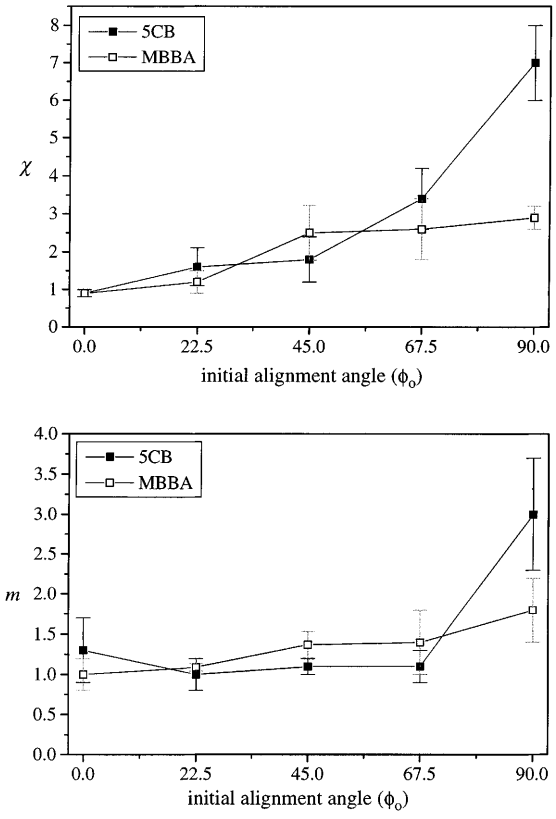

Fig. 8 Values of χ and m for 5CB and MBBA resulting from shearing a sample with varying initial alignment angle ϕ_0. As ϕ_0 increases from 0° to 90°, the slope of the director rotation transient (m) remains relatively constant until $\phi_0 = 90°$. The retardation of director rotation (χ) also increases with initial alignment angle

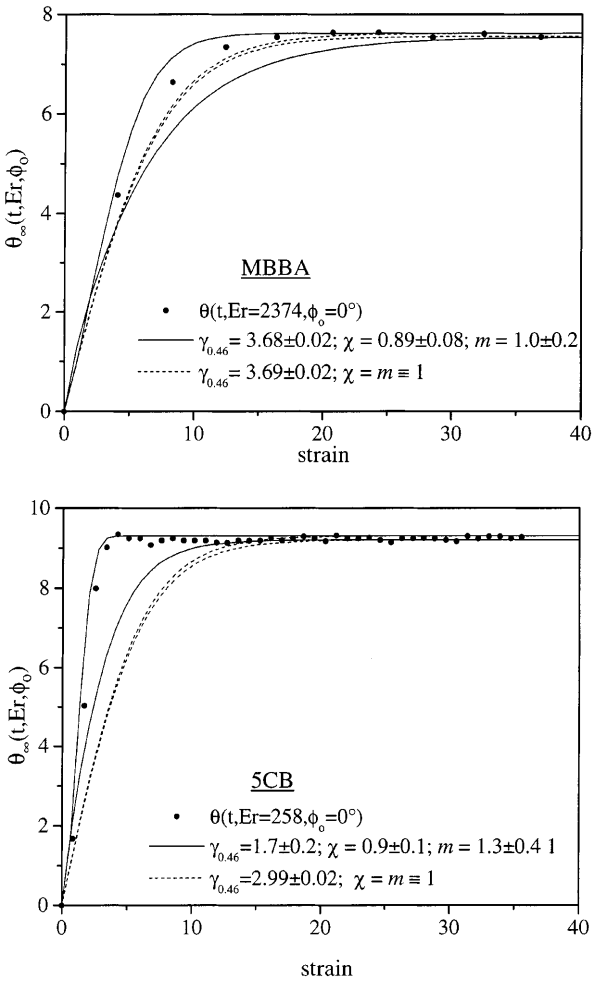

Fig. 9 Comparison of experimental data and fitted curves for MBBA and 5CB. The *points* are data from the highest shear rate used. The *solid lines* denote the limits of the curve fits for all shear rates using $\gamma_{0.46}$. The *dotted lines* are the limits based upon γ_L calculated from $\theta_\infty(\phi_0)$

The splay rotation of the director is governed by the ratio of the coefficients α_2 and α_3. These parameters act in the vorticity plane and should only affect the component of the director that is projected into that plane. With the initial alignment of the director increasing from $\phi_0 = 0°$ to $\phi_0 = 90°$, there is a corresponding decrease of the director component in the vorticity plane before the onset of shear. This results in a reduced splay rotation that is proportional to the vorticity plane director component. With increasing rotation into the direction of shear, the effect of α_2 and α_3 increases.

Table 1 Reported Leslie angles for 5CB and MBBA

5CB		MBBA	
Study	θ_∞ (25 °C)	Study	θ_∞ (25 °C)
This study	[a]9.23 ± 0.07°	This study	7.60 ± 0.09°
Skarp et al. (1979)	12.5°	Gasproux and Prost (1971)	[b]6.91°
Skarp et al. (1980)	[b]12.3 ± 0.7°	Gähwiller (1972)	6.5 ± 0.6°
Chmielewski (1986)	[b]10.1°	Pieranski and Guyon (1973)	[b]9.83°
Coles and Sefton (1987)	[b]11.8°	Wahl and Fischer (1973)	8.23°
Mather et al. (1996)	[b]9.6 ± 0.8°	Meiboom and Hewitt (1973)	[b]18.8°
		de Jeu (1978)	[b]6.0 ± 0.2°
		Kneppe et al. (1982)	6.9 ± 0.6°

[a] Low Ericksen numbers
[b] Values calculated from other material parameters provided in reference

Pieranski and Guyon (1974) discuss this phenomenon in more detail.

Another trend of the director splay is that the slope of the transient portion of the curve remains relatively constant up to at least $\phi_0 = 67.5°$. It then increases as $\phi_0 = 90°$ (Fig. 8, bottom).

The steady-state alignment angle $\theta_\infty(\mathrm{Er}, \phi_0)$ also increases with ϕ_0 as seen in Fig. 4. Even at high Ericksen numbers where $\theta_\infty(\mathrm{Er}, \phi_0) = \theta_\infty(\phi_0) = \theta_\mathrm{L}$, there is still an increase with θ_0. This finding is in agreement with the observations of Pieranski and Guyon (1974). If this effect is real then current theory does not explain the cause. If the effect is an artifact of the optical measurements, it may be due to the twist gradient and its effects on the resulting conoscopic image.

Rotation of the director splay during monodomain recovery was studied by normalizing the data in Fig. 6 and is shown in Fig. 10. The data is approximated by a single exponential decay, Eq. (11a).

$$\Theta = \frac{\theta_\mathrm{r}(t, \phi_0) - \theta_0}{\theta_\infty(\phi_0) - \theta_0} = \exp\left(\frac{t_1 - t}{\tau_\theta}\right) \tag{11a}$$

$$\tau_\theta = h^2 \frac{|\alpha_3|}{K_1} \frac{\left(\pi^2 \frac{\alpha_3 - \alpha_2}{|\alpha_3|} - (\pi^2 - 8)\frac{|\alpha_3|}{\eta_2}\right)}{\pi^4} \tag{11b}$$

$$\tau_\theta = \frac{h^2}{D_\mathrm{R}\pi^2}; \quad D_\mathrm{R} = \frac{K_1}{\eta_2} \tag{11c}$$

We obtained a characteristic relaxation time of $\tau_\theta = 36.2 \pm 0.4$ s. The characteristic relaxation time may be related to the viscous and elastic coefficients through the separate definitions of τ_θ in Eqs. (11b) and (11c). Equation (11b) is based upon Eq. (48) of Mather et al. (1996), and has been modified to reflect the planar alignment of our system. Using $h = 150$ μm and the viscosities η_2, α_2, and α_3 from Manneville and Dubois-Violette (1976), we obtain $K_1 = (4.9 \pm 0.1) \times 10^{-12}$ N which is close to the literature value of 6×10^{-12} N. The director diffusivity (D_R) may be obtained through Eq. (11c) of Müller et al. (1994). For our experiments, $D_\mathrm{R} = (5.89 \pm 0.08) \times 10^{-12}$ m^2 s^{-1} which is in excellent agreement with the literature value from Manneville and Dubois-Violette of 5.8×10^{-12} m^2 s^{-1}.

The director twist during monodomain recovery was studied by normalizing the data in Fig. 7. The results are displayed in Fig. 10 along with the splay relaxation. The influence of splay and the initial alignment angle (ϕ_0) on director twist recovery would involve K_2 and result in a more complex counterpart to Eqs. (11b) and (11c). The derivation of these equations is beyond the scope of this paper. Instead, a single exponential curve-fitting equivalent to Eq. (11) was used to extract a relaxation time (τ_ϕ) for the twist recovery.

$$\Phi = \frac{\phi_\mathrm{r}(t, \phi_0) - \phi_0}{\phi_\infty(\phi_0) - \phi_0} = \exp\left(\frac{t_1 - t}{\tau_\phi}\right) \tag{12}$$

Director recovery $\phi_\mathrm{r}(t,\phi_0)$ from $\phi_\infty(\phi_0)$ back to ϕ_0, shows a dependence on the initial alignment conditions while the splay recovery does not. As the difference between ϕ_0 and $\phi_\infty(\phi_0)$ increases, going from $\phi_0 = 0°$ to 90°, there is an increasing amount of twist in the system. This increase in twist energy was found to increase the recovery rate. The characteristic recovery times of director ϕ-rotation for $\phi_0 = 45°$ and 90° are $\tau_\phi = 120 \pm 3$ s, and $\tau_\phi = 48.0 \pm 0.8$ s respectively. The twist-driven recovery occurs more slowly than splay-driven recovery.

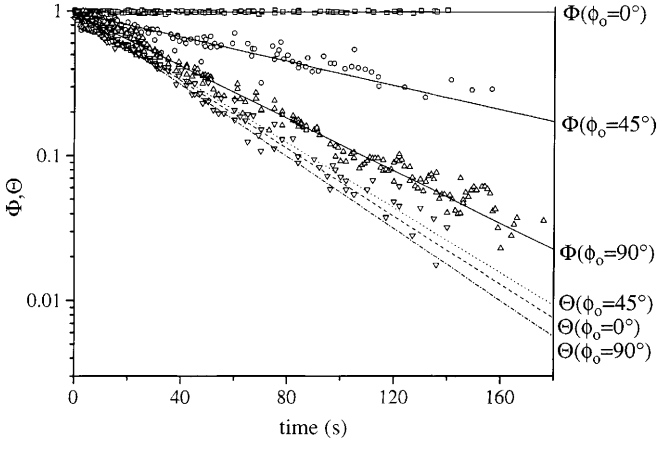

Fig. 10 Recovery in MBBA. The behavior of θ_r is relatively constant while the rate of rotation for ϕ_r increases with increasing ϕ_0. Data points are given for Φ, and for Θ ($\phi_0 = 0°$)

Conclusion

The initial director alignment is controlled by anchoring at the sample surface ($\theta_0 = 0°$; ϕ_0). Shear causes the molecular director to rotate. This introduces splay and twist near the anchoring walls. By separately observing director ϕ-rotation and θ-rotation, we have found clear evidence for an effect of initial alignment conditions upon director rotation dynamics during and after shear. An increase of the anchoring angle from $\phi_0 = 0°$ to 90° results in the following. During start-up of shear, the amount of strain necessary to achieve a steady-state alignment angle increases for both director twist and splay. In addition, there is a retardation period for director rotation which is nonexistent at $\phi_0 = 0°$ and grows as ϕ_0 increases from 0° to 90°.

The steady-state alignment is also dependent upon the direction of anchoring, ϕ_0. Increased ϕ_0 results in an increase in the steady-state alignment angle $\theta_\infty(\phi_0)$, which is defined as the Leslie angle when $\phi_0 = 0°$ (Fig. 4). This might however be an artifact of the conoscopic image.

When stopping the shear flow, LC molecules rotate back to alignment conditions which are governed by the strong boundary anchoring. The rate of twist recovery increases as the preferred alignment goes from the velocity axis to the vorticity axis. In contrast, the splay recovery shows no such ϕ_0 dependence and occurs faster than the twist recovery.

Acknowledgements We gratefully acknowledge financial support from the National Science Foundation through grant DMR9422180. We thank R. Larson who, as a member of the *Rheologica Acta* editorial board, conducted the anonymous review of the manuscript. We thank W. Burghardt and P. Mather for their helpful discussions and input, and Brett Van Horn for many discussions concerning the analysis of conoscopic experiments.

References

Bloss FD (1961) An introduction to the methods of optical crystallography. Hokt Rinehart and Wilson, New York

Born M, Wolf E (1969) Principles of optics, 4th edn. Pergamon Press, New York

Burghardt WR, Fuller GG (1990) Transient shear flow of nematic liquid crystals: Manifestations of director tumbling. J Rheol 34:959–992

Carlsson T (1984) Theoretical investigation of the shear flow of nematic liquid crystals with the Leslie viscosity $\alpha_3 > 0$: Hydrodynamic analogue of first order phase transitions. Mol Cryst Liq Cryst 104:307–334

Chang R (1973) The anisotropic refractive indices of aligned MBBA liquid crystal films. Mol Cryst Liq Cryst 28:1–8

Chmielewski AG (1986) Viscosity coefficients of some nematic liquid crystals. Mol Cryst Liq Cryst 132:339–352

Cladis PE (1972) New method for measuring the twist elastic constant K_{22}/χ_a and the shear viscosity γ_1/χ_a for nematics. Phys Rev Lett v28n25:1629–1631

Coles HJ, Sefton MS (1987) Pretransitional behaviour of the splay and twist elastic and viscosity constants for the nematic to smectic A phase transition in octyl cyanobiphenyl (8CB). Mol Cryst Liq Cryst Lett 4:123–130

Ericksen JL (1960) Anisotropic fluids. Arch Rat Mech Anal 4:231–237

Ericksen JL (1962) Hydrostatic theory of liquid crystals. Arch Rat Mech Anal 9:371–378

Gähwiller C (1972) Temperature dependence of flow alignment in nematic liquid crystals. Phys Rev Lett 28:1554–1556

Gasproux H, Prost J (1971) Détermination directe de l'anisotropie magnétique de crystaux liquides nématique. J Phys (Paris) 32:953–962

Gennes PE de, Prost J (1993) The physics of liquid crystals, 2nd edn. Clarendon Press, Oxford

Hongladarom K, Burghardt WR (1994) Measurement of the full refractive index tensor in sheared liquid crystalline polymer solutions. Macromolecules 27:483–489

Jeu WH de (1978) On the viscosity coefficients of nematic MBBA and the validity of the Onsager-Parodi relation. Phys Lett 69A:122–124

Karat PP, Madhusudana NV (1976) Elastic and optical properties of some 4′-*n*-alkyl-4-cyanobiphenyls. Mol Cryst Liq Cryst 36:51–64

Kirov N, et al (1980) Influence of a.c. electric field on infrared absorption spectra of liquid crystals and determination of orientational order parameter by infrared dichroism: II. Molecules with weak negative dielectric anisotropy. Mol Cryst Liq Cryst 58:299–310

Kneppe H, et al (1982) Rotational viscosity γ_1 of nematic liquid crystals. J Chem Phys 77:3203–3208

Larson RG (1999) The structure and rheology of complex fluids. Oxford University Press, New York

Leslie FM (1966) Some constitutive equations for anisotropic fluids. Q J Appl Math 19:357

Madhusudana NV, Pratibha R (1982) Elasticity and orientational order in some cyanobyphenyls. Mol Cryst Liq Cryst 89:249–259

Manneville P (1978) Non-linearities and fluctuations at the threshold of a hydrodynamic instability in nematic liquid crystals. J Phys (Paris) 39:911–925

Manneville P, Dubois-Violette E (1976) Shear flow instability in nematic liquids: Theory steady simple shear flows. J Phys (Paris) 37:285–296

Mather PT et al. (1996) Structural response of nematic liquid crystals to weak transient shear flows. J Rheol 39:627–648

Meiboom S, Hewitt RC (1973) Measurements of the rotational viscosity coefficients and the shear-alignment angle in nematic liquid crystals. Phys Rev Lett 30:261–263

Müller JA (1996) Optical rheometry of nematic liquid crystals with uniform molecular alignment. PhD Thesis, University of Massachusetts

Müller JA, et al (1994) Director dynamics of uniformly aligned solution of nematic liquid crystals in transient shear flow. Rheol Acta 33:473

Müller JA, et al (1996) Rotation of liquid crystalline macromolecules in shear flow and shear-Induced periodic orientation patterns. Rheol Acta 35:160–167

Nejoh H (1991) Liquid crystal molecule orientation on a polyimide surface. Surf Sci 256:94–101

Parodi O (1970) Stress tensor for a nematic liquid crystal. J Phys (Paris) 31:581

Pieranski P, Guyon E (1973) Shear-flow-induced transitions in nematics. Solid State Commun 13:435–437

Pieranski P, Guyon E (1974) Instability of certain shear flows in nematic liquids. Phys Rev A 9:404–417

Skarp K, et al (1979) Flow alignment in cyanobiphenyl liquid crystals. Phys Scr 19:339–342

Skarp K, et al (1980) Measurements of hydrodynamic parameters for nematic 5CB. Mol Cryst Liq Cryst 60:215–236

Srinivasaro M, Berry GC (1991) Rheo-optical studies on aligned nematic solutions of a rodlike polymer. J Rheol 35:379–397

Tobi AC (1956) A chart for measurement of optic axial angles. Am Mineral 41:516–519

Wahl J, Fischer F (1973) Elastic and viscosity constants of nematic liquid crystals from a new optical method. Mol Cryst Liq Cryst 22:359–373

Wahlstrom E (1969) Optical crystallography, 4th edn. Wiley, New York

Weibull W (1951) A statistical distribution function of wide applicability. J App Mech Sept:293–297

Weiss K, et al (1998) Molecular orientation at rubbed polyimine surfaces determined with X-ray absorption spectroscopy: relevance for liquid crystal alignment. Macromolecules 31:1930–1936